

Key words: *damage accumulation method, weight function method, multiaxial random loading, fatigue fracture planes*

ALEKSANDER KAROLCZUK^{*)}, EWALD MACHA^{**)}

CRITICAL AND FRACTURE PLANE ORIENTATIONS UNDER MULTIAXIAL CYCLIC AND RANDOM LOADING

The critical plane orientations determined with account for maximum value of energy density parameters and the weight function method were compared to experimental fatigue fracture plane orientations. Energy density parameters used in two multiaxial fatigue failure criteria, i.e. (i) criterion of the maximum normal strain energy density on the critical plane and (ii) criterion of the maximum shear strain energy density on the critical plane were employed. In the other method, the weight functions were formed on the basis of energy parameters. These two methods were verified by experimental tests of 18G2A steel. The material was subjected to cyclic and random bending, torsion and combined bending with torsion with different coefficients of cross correlation between normal and shear stresses. The calculated results are satisfactory for both methods.

NOMENCLATURE

τ, γ	shear stress and strain, respectively,
σ, ε	normal stress and strain, respectively,
W	strain energy density parameter,
$\lambda_\sigma = \tau_{\max}/\sigma_{\max}$	stress ratio,
$r_{\sigma\tau}, \delta$	cross correlation coefficient and phase shift between stresses σ and τ , respectively,
m_σ, m	coefficients depending on the slope of the fatigue curve for fully reversed, axial and torsion loading, respectively,

^{*)} *Technical University of Opole, Faculty of Mechanical Engineering, ul. Mikotajczyka 5, 45-271 Opole, Poland; E-mail: karol@po.opole.pl*

^{**)} *Technical University of Opole, Faculty of Mechanical Engineering, ul. Mikotajczyka 5, 45-271 Opole, Poland; E-mail: emac@po.opole.pl*

σ_{af}, τ_{af}	fatigue limit for fully reversed axial and torsion loading, respectively,
b, c	fatigue strength exponent and fatigue ductility exponent, respectively,
σ'_f	fatigue strength coefficient,
R_e, R_m	yield stress and ultimate strength, respectively,
E, G	Young and Kirchhoff elastic moduli,
ν	Poisson ratio,
n', K'	exponent and coefficient of cyclic hardening model, respectively,
N_0	number of cycles at fatigue limit σ_{af} or τ_{af} ,
α	angle between specimen axis and vector \vec{n} ,
φ, θ, ψ	Euler's angles,
W, sgn	weight and signum function, respectively.
	Indices and others,
a	amplitude,
1, 2, 3	principal values from maximum to minimum, respectively,
af	fatigue limit,
exp, cal	experimental and calculated value, respectively,
n	in plane with normal \vec{n} ,
s	in direction \vec{s} ,
ns	in direction \vec{s} on plane with normal \vec{n} ,
Δ	range,
\wedge	expected value.

1. Introduction

The idea of critical plane seems to be dominating in modern literature on fatigue life determination under multiaxial loading. Many fatigue criteria are based on the concept of the critical plane. In these criteria, it is assumed that loading (stress, strain or energy parameters) acting in the plane where fatigue crack may grow are responsible for fatigue of the material. The proper orientation of that plane (critical plane) in fatigue criteria based on the critical plane concept must be established for fatigue life calculation. Stanfield [1] was the first researcher who proposed to apply the critical plane for description of multiaxial fatigue in 1935. This concept has been more and more popular since this date. The damage accumulation method is often used for determination of the critical plane orientation. In this method, the plane of maximum damage degree is searched for. A damage degree in the critical plane depends, among other things, on selection of the fatigue effort criterion. In the case of non-proportional, especially random loading, a search for the

critical plane with the damage accumulation method is time consuming, because it needs iterative calculation of a damage degree on many planes. Hence, the critical plane orientation is very often defined as a plane experiencing the maximum value of the chosen damage parameter. The weight function is another method of calculation of the critical plane orientation [2], [3], [4], [5]. Multiaxial fatigue tests prove that fatigue fracture plane orientations refer to the principal stress or strain directions to a large degree [6], [7], [8], [9], [10], [11]. However, numerous models of fatigue crack initiation and propagation for multiaxial loading do not take into account the change of the principal stress axes. When principal axes directions rotate, then the greater number of the differently oriented crystallographic slip planes is activated by the maximum shear stress τ_{13} , in comparison to the case of loading with stable directions of principal axes. Hence, it may be assumed that the fatigue fracture plane orientation is the averaged orientation among all the activated slip planes. Averaged principal stress directions should be determined, and the averaging procedure could be carried out to estimate the critical plane orientation. Weight function method consist in averaging process of instant principal axes directions ($1(t)$, $2(t)$, $3(t)$) weighted through suitable function. Principal axes direction are determined in each time instant t by three Euler angles which are taken in the averaged process. When the averaged principal axes direction ($\hat{1}, \hat{2}, \hat{3}$) are established, then the critical plane orientation is determined in relation to their directions. It means that the critical plane orientation may be assumed, e.g. to be perpendicular to the averaged principal maximum stress direction $\hat{1}$ (for materials in brittle state), or coincided with averaged maximum shear stress plane, i.e. the plane $\hat{1}\hat{3}$ (for materials in ductile state). Orientations of the fatigue fracture planes under multiaxial random loading have not been well evidenced in literature. The aim of this paper is to verify efficiency of determination of the fatigue fracture plane orientations (assumed as the critical planes) with the maximum value of the normal or shear strain energy density parameter and weight function method under multiaxial random loading on the basis of experimental data.

3. Experiments

Smooth specimens (Fig. 1) made of 18G2A steel were tested under high-cycle regime. The specimens were subjected to cyclic and random loading with zero mean value (Fig. 2). Static properties of the steel tested are the following: $R_e = 357$ MPa; $R_m = 535$ MPa; $E = 210$ GPa; $\nu = 0.3$. Chemical composition (in %) is: C = 0.21; Mn = 1.46; Si = 0.42; P = 0.019;

$S = 0.046$; $Cr = 0.09$; $Cu = 0.17$; $Ni = 0.04$; (remaining Fe). Cyclic parameters of the steel are described by the following parameters: $\sigma_r' = 782$ MPa; $b = -0.118$; $m_\sigma = m_\tau = 8.2$; $c = -0.410$; $K' = 869$ MPa; $n' = 0.287$; $\sigma_{of} = 204$ MPa; $\tau_{of} = 170$ MPa, $N_0 = 1120000 \cdot \text{cycles}$.

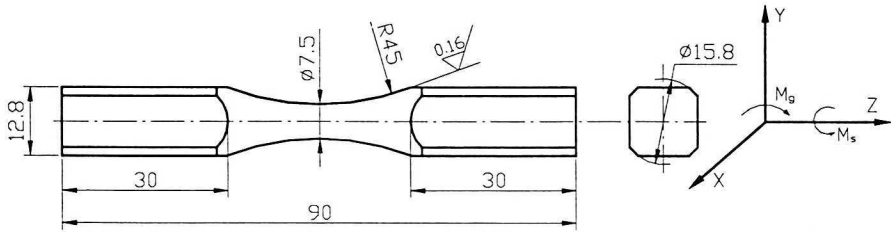


Fig. 1. Specimen geometry

Under cyclic loading, the tests were carried out for sinusoidal proportional courses and non-proportional courses with the phase shift $\delta = \pi/2$ for different ratios of amplitudes of shear and normal stresses $\lambda_\sigma = \tau_a/\sigma_a$ (Table 1). Normal stresses $\sigma(t)$ from bending and shear stresses $\tau(t)$ from torsion were calculated from instantaneous values according to were calculated using elastic beam theory.

$$\sigma(t) = \sigma_a \sin(2\pi ft), \quad \tau(t) = \tau_a \sin(2\pi ft - \delta), \quad (1)$$

Under random loading, the specimens were subjected to random bending, torsion and combined bending with torsion with three coefficients of cross correlations between normal and shear stresses ($\nu_{\sigma\tau} = 0.0, 0.5, 1.0$). Loading courses with normal probability distributions (Fig. 3) and narrow frequency bands (Fig. 4) were generated on the computer as one block. The block lasted 33 minutes and 20 seconds. The block was repeated up to the specimen failure. An exemplary part of random stress histories is shown in Fig. 2. The fatigue tests were done for different ratios of the maximum shear and normal stresses $\lambda_\sigma = \tau_{\max}/\sigma_{\max}$ (Table 1). Fatigue lives and positions of crack lines were determined with the angle α_{exp} (Fig. 5). The crack directions were determined on the basis of photographs of the specimen surfaces analyzed with use of an optical microscope combined with a computer (magnification $60\times$). As a result, we obtained a picture of a surface fragment 1.8×1.8 mm with a resolution 167×167 pixels per one mm^2 . The points representing fatigue crack were approximated by a straight line with the least square method. The line slope coefficient was used to determine the angle between the vector normal to the line crossing the crack and the specimen axis α_{exp} .

(Fig. 5, (a), (b)). Table 1 contains the experimental mean values of the angles of the crack line slopes $\hat{\alpha}_{exp}$ and the calculated confidence intervals (assuming normal distribution of measurements of α_{exp}) with probability 0.99. In the case of loading 2 and 8 (Table 1), one dominating direction and some other directions of cracking were observed. The angles $\hat{\alpha}_{exp}$ determining additional crack directions are given in the brackets.

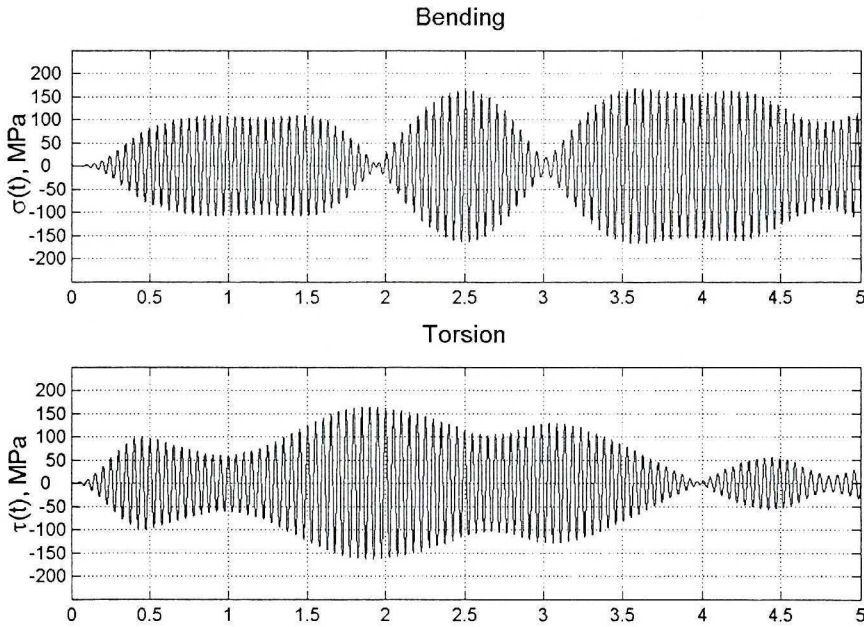


Fig. 2. Fragments of stress histories for random loading

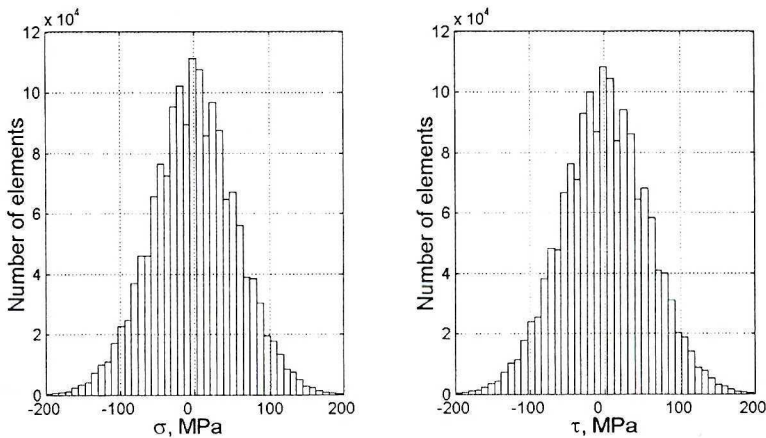


Fig. 3. Histograms of bending and torsion stresses, σ and τ

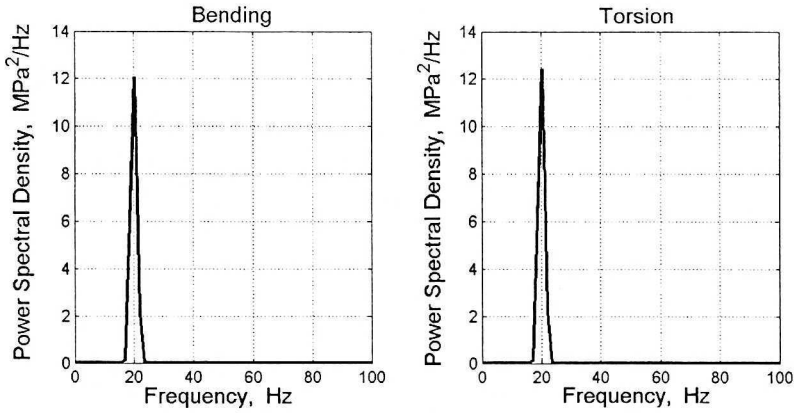


Fig. 4. Power spectral density function for bending and torsion

Table 1.

Average values of experimental angles α_{exp}

No	Number of specimen	$r_{\sigma\tau}$ –	λ_{σ} –	α_{exp} [°]	$\Delta\alpha_{\text{exp}}$ [°]
1	2	3	4	5	6
Random					
1	10	Bending	0	1.5	2.2
2	5	Torsion	∞	43.6 (90)	8.7
3	8	1.0	0.50	20.5	9.4
4	5	1.0	1.00	31.4	9.8
5	5	0.5	0.54	16.2	7.7
6	5	0.5	0.97	28.2	8.1
7	6	0.0	0.56	4.8	7.9
8	5	0.0	0.97	31.2 (0/90)	9.9
Cylik					
9	7	1.0	0.34	18.1	4.7
10	9	1.0	0.48	21.9	6.3
11	8	1.0	0.72	26.5	11.2
12	8	0.0	0.34	12.3	11.7
13	6	0.0	0.49	8.4	5.5
14	7	0.0	0.71	10.2	13.3

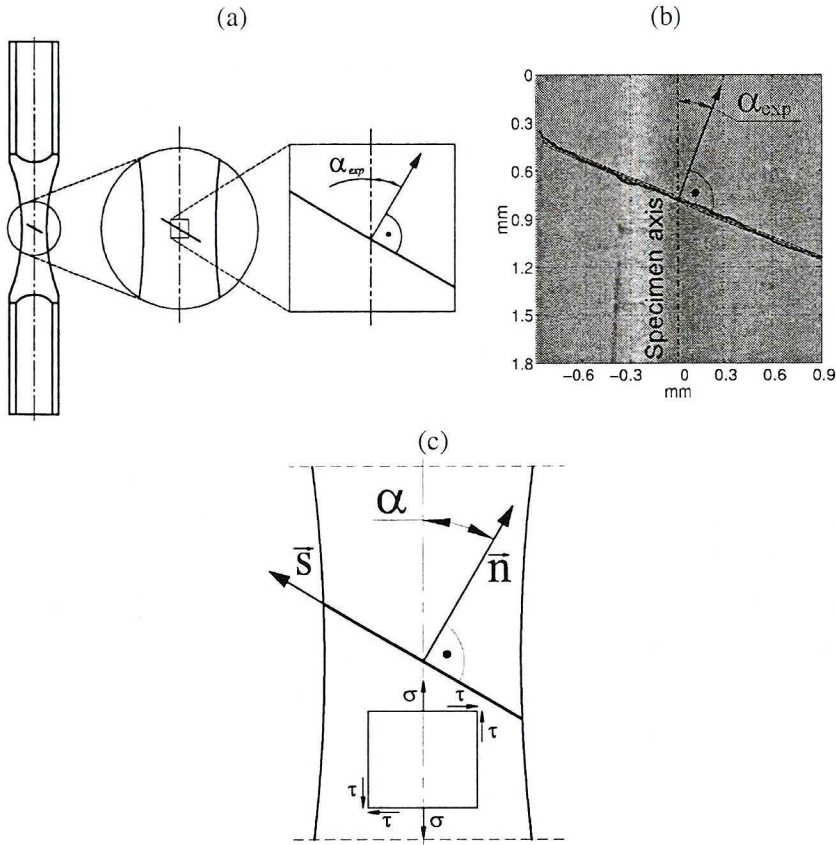


Fig. 5. (a), (b) – scheme of measurement of angle α_{exp} , (c) – definition of angle α

4. Strain energy density parameters

Two energy density parameters used in multiaxial fatigue criteria were applied for calculation of the critical plane orientations, i.e. the criterion of maximum parameter of normal strain energy density in the critical plane, $W_{n,max}$ and the criterion of maximum parameter of shear strain energy density in the critical plane, $W_{ns,max}$. Normal and shear stresses for any orientation of the plane (Fig. 5, (c)) in the plane stress state can be expressed versus angle α as:

$$\sigma_n(t) = \sigma(t) \cos^2 \alpha + \tau(t) \sin 2\alpha, \quad \tau_{ns}(t) = \tau(t) \cos 2\alpha - \frac{1}{2} \sigma(t) \sin 2\alpha. \quad (2)$$

Similar can be done for strains in the elastic range:

$$\varepsilon_n(t) = \frac{\sigma(t)}{E} (\cos^2 \alpha - \nu \sin^2 \alpha) + (1 + \nu) \frac{\tau(t)}{E} \sin 2\alpha, \quad (3)$$

$$\varepsilon_{ns}(t) = \frac{(1 + \nu)}{E} \left[\tau(t) \cos 2\alpha - \frac{1}{2} \sigma(t) \sin 2\alpha \right]. \quad (4)$$

Using Eqs. (2)–(4), it was possible to calculate the parameters of normal strain energy density $W_n(t)$ and shear strain energy density $W_{ns}(t)$ [12] in the plane determined by angle α :

$$W_n(t) = \frac{1}{2} \sigma_n(t) \varepsilon_n(t) \frac{\text{sgn}[\sigma_n(t)] + \text{sgn}[\varepsilon_n(t)]}{2}, \quad (5)$$

$$W_{ns}(t) = \frac{1}{2} \tau_{ns}(t) \varepsilon_{ns}(t) \frac{\text{sgn}[\tau_{ns}(t)] + \text{sgn}[\varepsilon_{ns}(t)]}{2}. \quad (6)$$

In the considered criteria, the critical plane is the plane of orientation determined by angle α_{cal} , where the analyzed parameter reaches the maximum value. The experimental data for 18G2A steel and the results of calculations of the angle determining the fatigue fracture plane position with the maximum value of two parameters (5)–(6) are contained in Table 2. In the square brackets there are intervals of the angle values for the damage parameters reduced by 1%. Thus, the intervals of the critical plane positions with the highest probability of occurrence were obtained.

5. Weight function method

The weight functions were applied in the averaging process of principal axis directions of stresses or strains in order to point out the positions strongly influencing the fatigue damage process. Three Euler angles φ , θ , ψ , described in [2], [3] were subjected to the weighted averaging process. The average weighted Euler angles are calculated from:

$$\hat{\varphi} = \frac{1}{W} \sum_{k=1}^N \varphi(t_k) W(t_k), \quad \hat{\theta} = \frac{1}{W} \sum_{k=1}^N \theta(t_k), \quad \hat{\psi} = \frac{1}{W} \sum_{k=1}^N \psi(t_k) W(t_k), \quad (7)$$

where: $\mathbf{w} = \sum_{k=1}^N W(t_k)$ – sum of weights.

Weight 1

$$W_1(t) = \begin{cases} 0 & \text{for } W_n(t) < cW_{of,n} \\ \left(\frac{W_n(t)}{cW_{of,n}} \right)^{\frac{m_\sigma}{2}} & \text{for } W_n(t) \geq cW_{of,n} \end{cases} \quad (8)$$

Weight 1 is based on the parameter of normal strain energy density (5). Parameter of normal strain energy density is computed in each time instant on the plane where product of normal stress $\sigma_n(t)$ and normal strain $\varepsilon_n(t)$ including signum function reaches the maximum value. It means that the orientation of that plane may change at each time instant but the critical plane orientation is the weighted average position of these planes. The weight 1 includes only the positions of principal axes where the parameter of normal strain energy density $W_n(t)$ is higher than the product of coefficient c ($c = 0.25$) and the fatigue limit expressed as the normal strain energy density $W_{of,n} = \sigma_{af}^2 / (2E)$ (for N_0 cycles). Hence, the normal strain energy density $W_n(t)$ taken into consideration in weight 1 is always positive.

Weight 2

$$W_2(t) = \begin{cases} 0 & \text{for } W_{ns}(t) < cW_{of,ns} \\ \left(\frac{W_{ns}(t)}{cW_{of,ns}} \right)^{\frac{m_\tau}{2}} & \text{for } W_{ns}(t) \geq cW_{of,ns} \end{cases} \quad (9)$$

Weight 2 is based on the same rules as the previous one, however, it does not use the normal strain energy density, but the shear strain energy density. The parameter of shear strain energy density $W_{ns}(t)$ is calculated at any time instant in the plane of the maximum product of shear stress $\tau_{ns}(t)$ and shear strain $\varepsilon_{ns}(t) = \gamma_{ns}(t)/2$. Weight 2 includes only those positions of the principal axes where the parameter of shear strain energy density $W_{ns}(t)$ is higher than the product of coefficient c and the fatigue limit expressed as shear strain energy $W_{of,ns} = \tau_{of}^2 / (4G)$. After determining the averaged Euler angles, the elements of the direction cosines matrix of the averaged principal stress directions are calculated. Table 2 contains the experimental data and the results of calculations.

Angle $\hat{\alpha}(W_1)$ is the angle between the averaged direction of the maximum principal stress \hat{I} and the specimen axis. Angle $\hat{\alpha}(W_2)$ is the angle between the averaged direction of the maximum shear stress τ_{13} in the plane $\hat{I}\hat{3}$ and the specimen axis.

6. Calculated and experimental results

Figs 6–9 show the most characteristic time histories in one loading cycle from the simulated stress states, namely for the parameter of normal strain energy density, W_n and shear strain energy density W_{ns} for different angles α . The maximum values determine the critical plane position α_{cal} . In the figures, the level lines 0.99, 0.9, 0.8, 0.7 etc. were shown for the maximum value. Also a projection of of 3D surface was done on the vertical wall in order to reach the maximum parameters for each value of angle α .

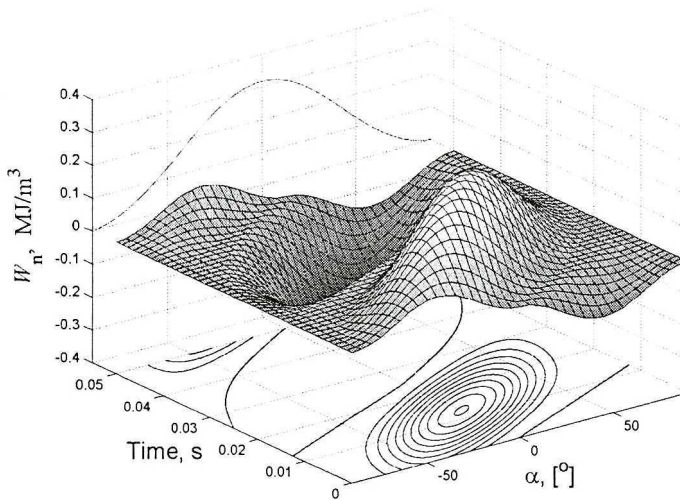


Fig. 6. Histories of the normal strain energy density parameter $W_n(t, \alpha)$ in a loading cycle for different angles α for the stress amplitude ratio $\lambda_\sigma = 0.49$ ($\sigma_n = 367$ MPa) and stress phase shift $\delta = \pi/2$

For the amplitude ratio $\lambda_\sigma = 0.49$ and phase shift of stresses $\delta = \pi/2$, the parameter of shear strain energy density determines the position of the critical plane for angle $\alpha_{cal} = 45^\circ$, but it is important that the maximum values of $W_{ns}(t, \alpha)$ (from 1 to 0.99) occur in very wide ranges of angle α_{cal} (from 30.1° to 59.9°) (Fig. 7). This criterion, for the amplitude ratio $\lambda_\sigma = 0.50$ and at the phase shift $\delta = \pi/2$, reaches the maximum amplitudes in all the range of angle α . The other characteristic case, according to the normal strain energy density

parameter $W_n(t, \alpha)$, is loading at the amplitude ratio $\lambda_\sigma = 0.71$ and the stress phase shift $\delta = \pi/2$. For such loading values, the parameter of normal strain energy density $W_n(t, \alpha)$ reaches its maximum for angle $\alpha_{\text{cal}} = 23.0^\circ$. However, this parameter does not strongly change in the interval from 14.6° to 28.7° (Fig. 8).

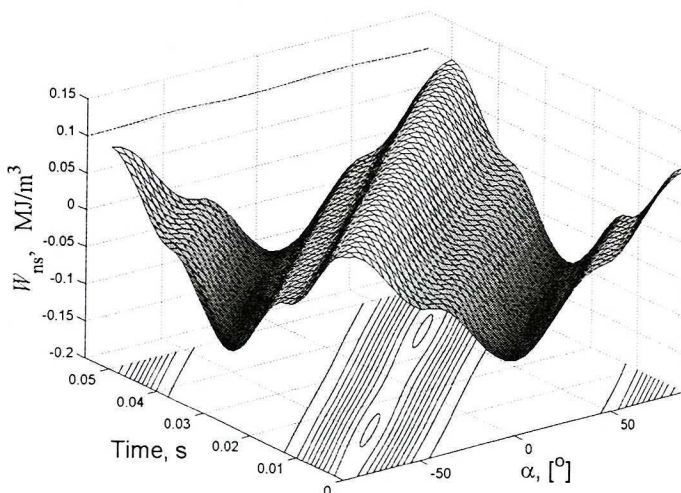


Fig. 7. Histories of the shear strain energy density parameter $W_{ns}(t, \alpha)$ in a loading cycle for different angles α for the stress amplitude ratio $\lambda_\sigma = 0.49$ ($\sigma_a = 367$ MPa) and stress phase shift $\delta = \pi/2$

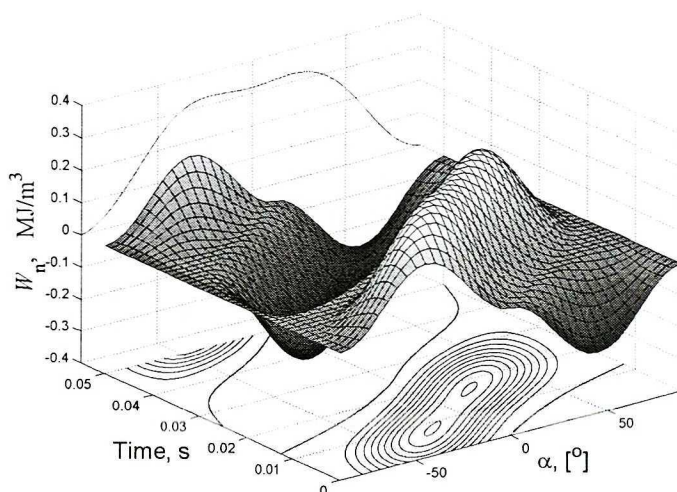


Fig. 8. Histories of the parameter of normal strain energy density $W_n(t, \alpha)$ in a loading cycle for different values of α for the stress amplitude ratio $\lambda_\sigma = 0.71$ ($\sigma_a = 367$ MPa) and stress phase shift $\delta = \pi/2$

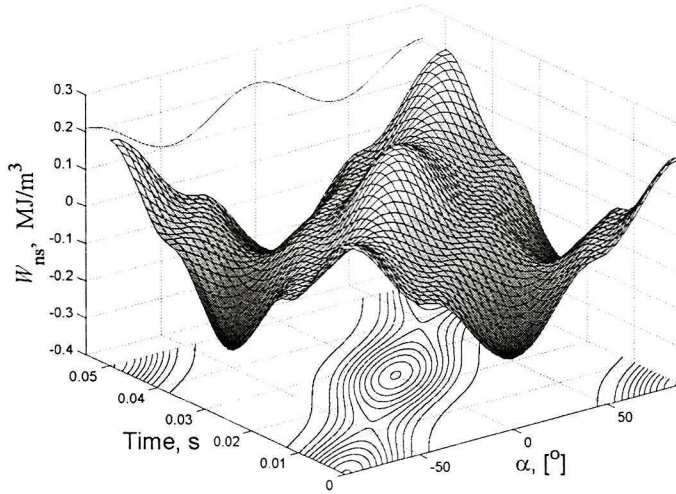


Fig. 9. Histories of the parameter of shear strain energy density $W_{ns}(t, \alpha)$ in a loading cycle for different values of α for the stress amplitude ratio $\lambda_{\sigma} = 0.71$ ($\sigma_n = 367$) MPa and stress phase shift $\delta = \pi/2$

Figs. 10–13 show the histograms of two parameters, $W_n(\alpha)$ and $W_{ns}(\alpha)$ for different orientations of the plane determined by angle α . These figures do not include full ranges of the considered parameters because only frequencies of occurrence of the maximum values are interesting for us. Thus, the histograms show frequencies of occurrence of instantaneous values from 1 to 0.5 of the maximum value of the considered parameter.

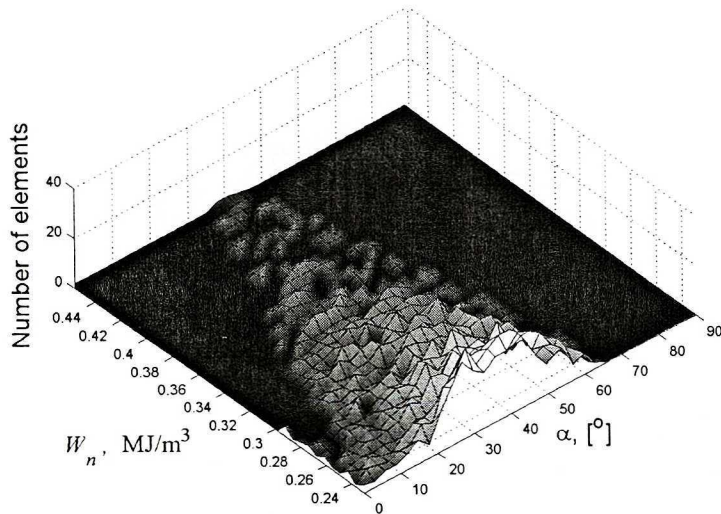


Fig. 10. Histograms of the parameter of normal strain energy density $W_n(t, \alpha)$ in a block of random loading for different angles α for the ratio of maximum stresses $\lambda_{\sigma} = 0.97$ ($\sigma_{\max} = 367$ MPa) and the cross correlation coefficient $r_{\sigma\epsilon} = 0.0$

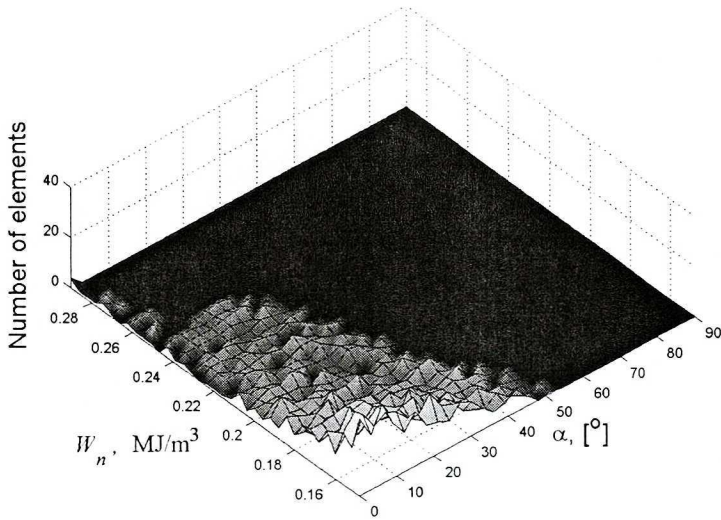


Fig. 11. Histograms of the parameter of normal strain energy density $W_n(t, \alpha)$ in a block of random loading for different values of angle α for the ratio of maximum stresses $\lambda_\sigma = 0.56$ ($\sigma_{\max} = 367$ MPa) and the cross correlation coefficient $r_{\sigma\tau} = 0.0$

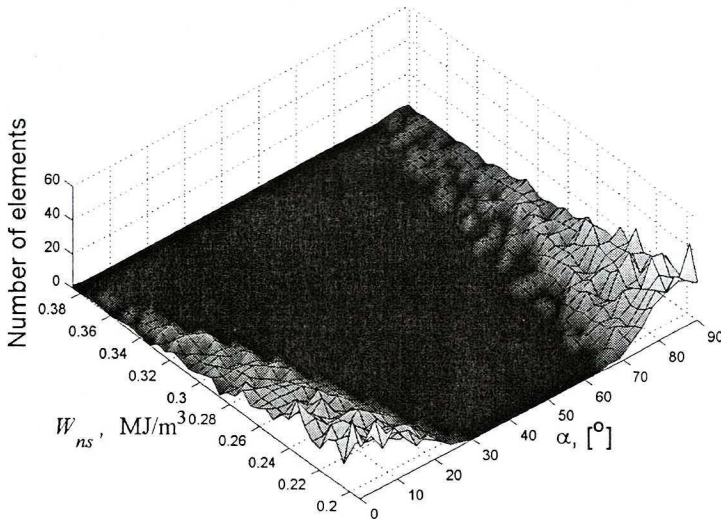


Fig. 12. Histograms of the parameter of shear strain energy density $W_{ns}(t, \alpha)$ in a block of random loading for different angles α for the ratio of maximum stresses $\lambda_\sigma = 0.97$ ($\sigma_{\max} = 367$ MPa) and the cross correlation coefficient $r_{\sigma\tau} = 0.0$

In the criterion of maximum parameter of shear strain energy density $W_{ns}(\alpha)$ (for $\lambda_\sigma = 0.56$ and $r_{\sigma\tau} = 0.0$) there is no one dominating plane position (Fig. 13). It can be joined with the case of cyclic loading for $\lambda_\sigma = 0.5$ and the phase shift $\delta = \pi/2$, where for each plane position (angle α) we can observe the same maximum amplitude of the parameter of shear strain energy density.

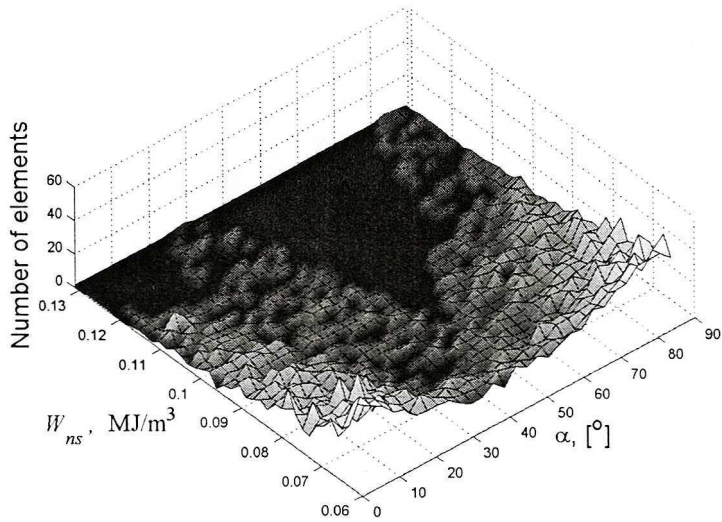


Fig. 13. Histograms of the parameter of shear strain energy density $W_{ns}(t, \alpha)$ in a block of random loading for different angles α for the ratio of maximum stresses $\lambda_\sigma = 0.56$ ($\sigma_{max} = 367$ MPa) and the cross correlation coefficient $r_{\sigma\tau} = 0.0$

It results from the tests done by many authors [13], [16] that under combination of bending with torsion and tension-compression with torsion and under proportional loading, orientation of the fatigue fracture plane in steels and cast irons coincides with the direction of maximum normal stress, independently on the stress ratio λ_σ . Under non-proportional loading, the fatigue fracture plane position depends on the ratio of amplitudes or maximum stresses λ_σ and on the cross correlation coefficient. Fig. 14 presents histories of the parameters applied for estimation of the critical plane position for two cases in a proportional loading cycle $\lambda_\sigma = 0.34$ and $\lambda_\sigma = 0.72$. The extremes of parameters of normal strain energy density $W_n(t)$ and shear strain energy density $W_{ns}(t)$ occur at the same time instant but for different angles α ($\alpha = 17.0^\circ$ for $\lambda_\sigma = 0.34$ and $\alpha = 27.5^\circ$ for $\lambda_\sigma = 0.72$; Fig. 14). Under proportional loading, the extremes of parameters of strain energy density $W_n(t)$, $W_{ns}(t)$ and the weight functions are distinct, and it results in a little scatter of experimental results of angle α_{exp} . The calculation results for the crack line slope obtained with the weight function and damage accumulation methods agree with the experimental results of angle $\hat{\alpha}_{exp}$ under proportional loading. The crack line directions for such loading correspond to Mode I. Thus, the weight functions and the criteria based on the parameters influencing occurrence of Mode I seem to be the best ones.

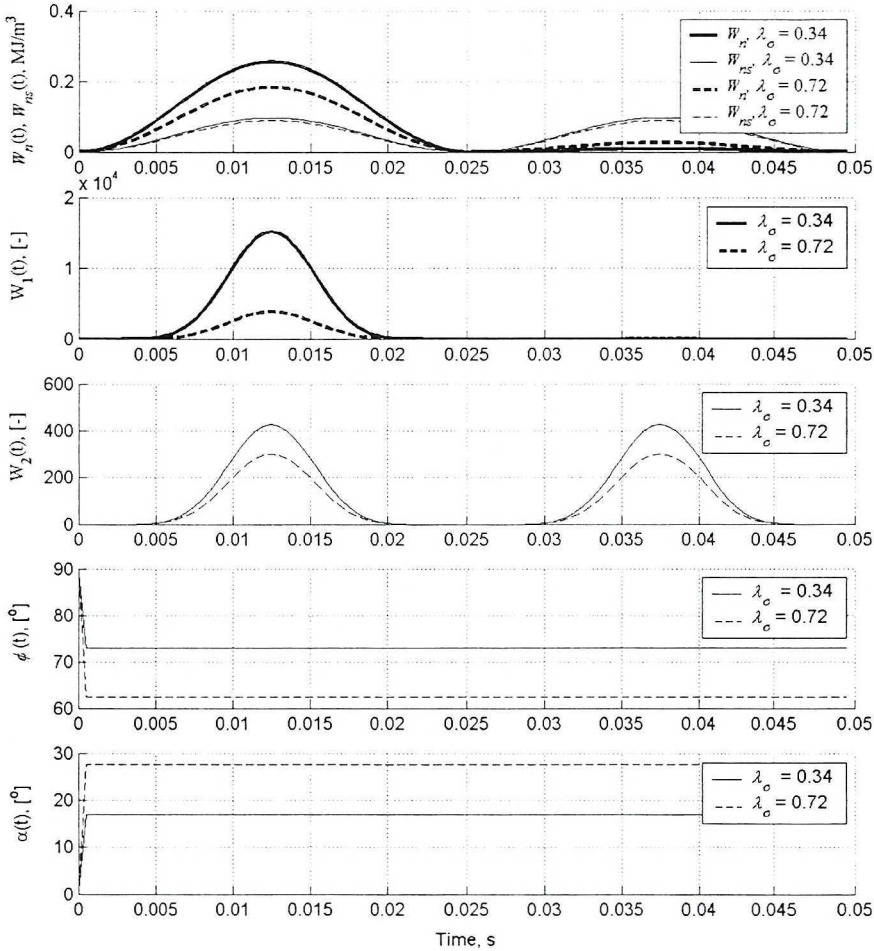


Fig. 14. Histories of the energy parameters $W_n(t)$, $W_{ns}(t)$, weight functions $W_1(t)$, $W_2(t)$, Euler angle $\varphi(t)$ and angle between the vector determining the stress principal direction and the specimen axis $\alpha(t)$ in a proportional loading cycle ($\delta = 0$)

The parameter histories under non-proportional loading ($\delta = \pi/2$) and for the ratio of stress amplitudes $\lambda_\sigma = 0.71$ and $\lambda_\sigma = 0.34$ are shown in Fig. 15. Under such loading, the extremes of the parameters of normal strain energy density $W_n(t)$ and the shear strain energy density $W_{ns}(t)$ do not occur at the same time (Fig. 15). In the case of the ratio of stress amplitude $\lambda_\sigma = 0.71$, it is difficult to observe any distinct extreme of the parameter of normal strain energy density versus angle α . History of the parameter of normal strain energy density takes the maximum value at a long time interval (0.005 s ÷ 0.02 s) at a changing angle $\alpha(t)$ of the maximum principal stress position. The distinct extreme can be observed for the parameter of shear strain energy density. Thus, mode II occurs in spite of normal strain energy

density higher than shear strain energy density. This conclusion can be proved by observations of fatigue crack lines (Fig. 16). Table 2 contains the experimental data and calculation results for the angle determining the fatigue fracture plane position obtained with the damage accumulation method and the weight function method. The bold letters mean the calculation results for the angle of the crack line slope, included in 99% confidence interval determined according to the experimental data or the results where the absolute value of difference between the calculated and experimental angles is less than 6° . Moreover, the calculated and experimental angles α according to mode II are underlined.

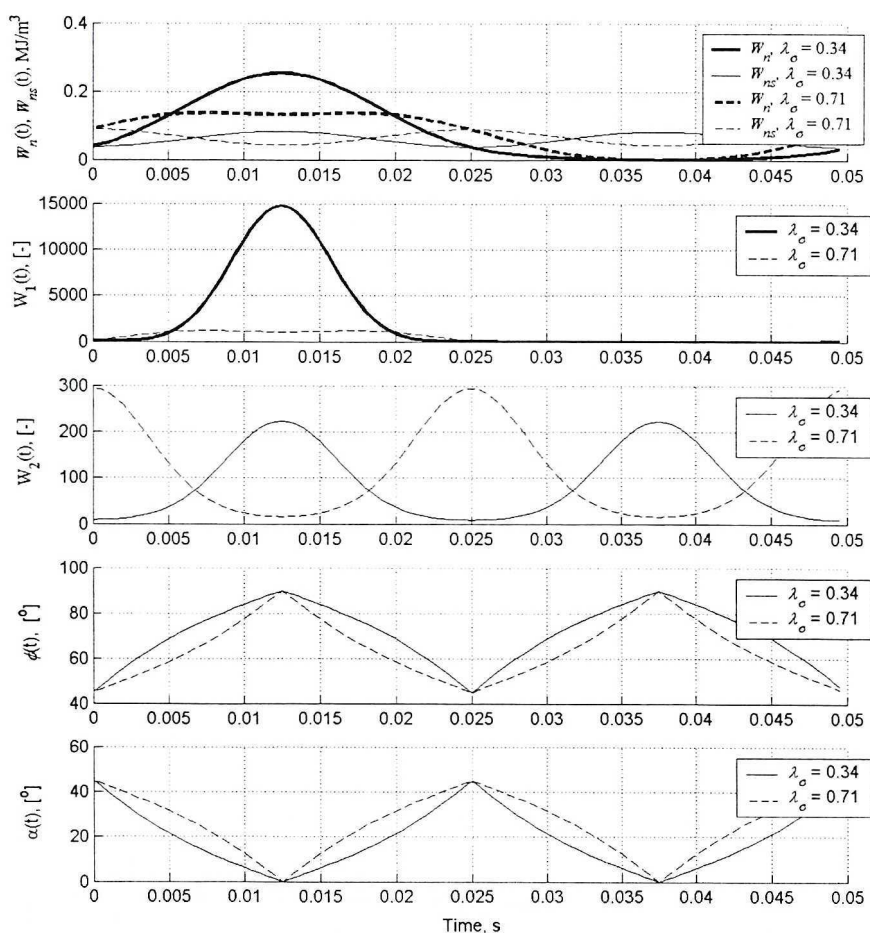


Fig. 15. Histories of energy parameters $W_n(t)$, $W_{ns}(t)$, weight functions $W_1(t)$, $W_2(t)$, Euler angle $\varphi(t)$ and the angle between the vector determining the principal stress direction and the specimen axis $\alpha(t)$ in a non-proportional loading cycle ($\delta = \pi/2$)

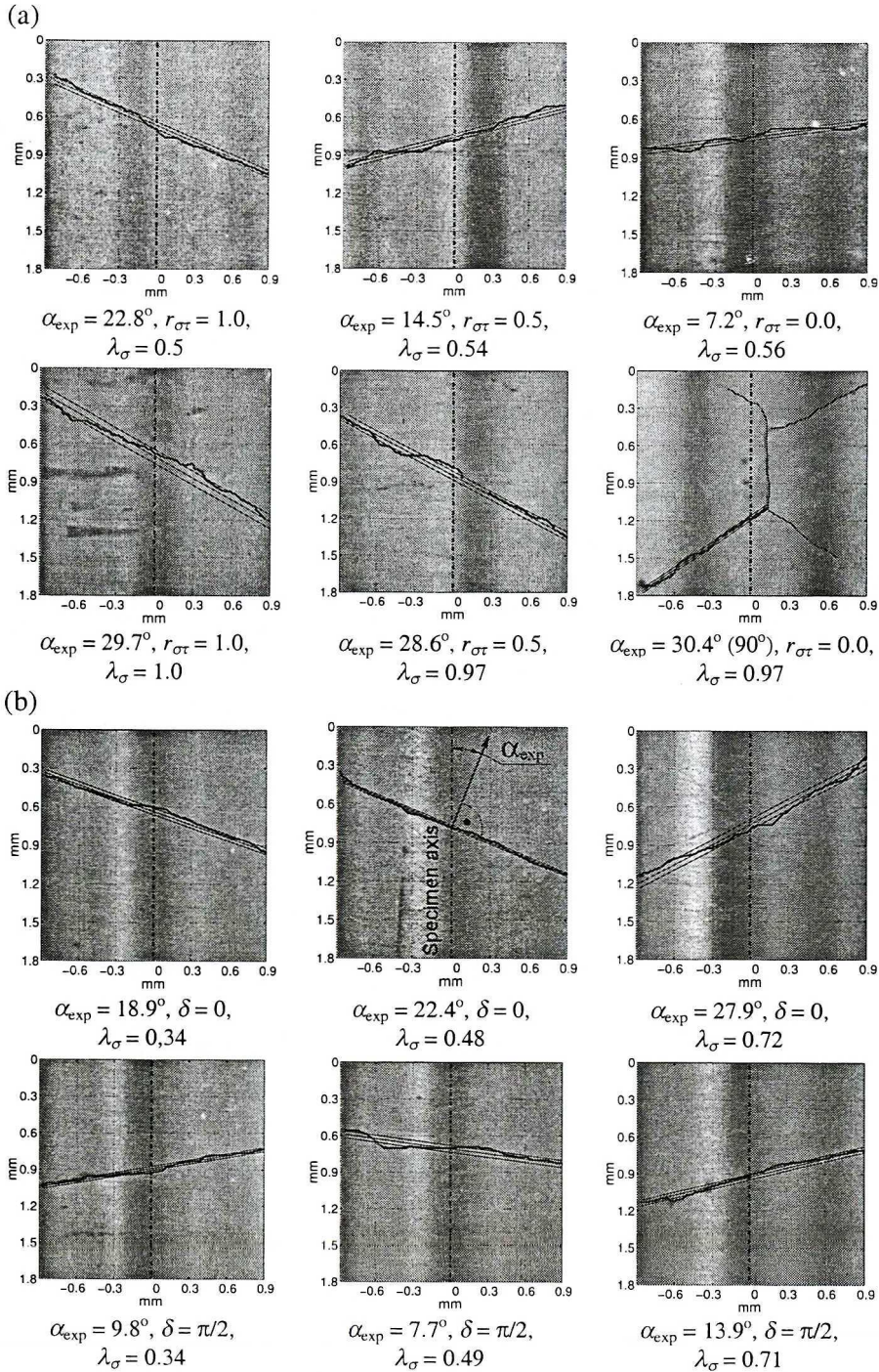


Fig. 16. The chosen photos of fatigue crack lines, a – random loading, b – cyclic loading

Table 2.
Experimental data and calculation results for the angle determining the fatigue fracture plane position with the damage accumulation and weight function methods

No	$r_{\sigma\tau}$ [-]	λ_{σ} [-]	$\hat{\alpha}_{exp}$ [°]	$\alpha_{cal}(W_{n,max})$ [°]	$\alpha_{cal}(W_{ns,max})$ [°]	$\hat{\alpha}(W_1)$ [°]	$\hat{\alpha}(W_2)$ [°]
Random							
1	– (Bending)	0	1.5 [0.38–2.57]	0.0 [0.0–3.7]	45.0 [42.2–47.8]	0.0	<u>0.1</u>
2	– (Torsion)	∞	43.6 (90) [39.2–47.9]	45.0 [42.2–47.8]	<u>0.0</u> [0.0–2.8]	45.0	<u>0.0</u>
3	1.0	0.50	20.5 [15.8–25.2]	22.5 [19.0–26.0]	67.5 [70.0–75.0]	22.5	<u>22.5</u>
4	1.0	1.00	31.4 [27.5–37.3]	31.5 [28.5–35.0]	76.5 [74.0–79.5]	31.7	13.3
5	0.5	0.54	16.2 [12.3–20.0]	23.5 [20.0–28.0]	71.0 [68.3–73.8]	20.4	<u>18.6</u>
6	0.5	0.97	28.2 [24.2–32.3]	33.0 [30.0–36.0]	86.0 83.3–89.3]	33.6	8.1
7	0.0	0.56	4.8 [0.8–8.7]	0.0 [0.0–0.8]	84.2 [81.8–87.3]	17.1	13.9
8	0.0	0.97	31.2 (0/90) [26.3–36.2]	41.7 [38.5–44.5]	86.8 [84.3–89.5]	35.9	<u>4.1</u>
Cyclic							
9	1.0 ($\delta = 0$)	0.34	18.1 [15.7–20.4]	17.0 [13.4–20.6]	62.0 [59.2–64.8]	17.0	28.0
10	1.0 ($\delta = 0$)	0.48	21.9 [18.8–25.1]	21.9 [18.4–25.4]	66.9 [64.1–69.7]	21.9	<u>23.1</u>
11	1.0 ($\delta = 0$)	0.72	26.5 [20.9–32.1]	27.5 [24.2–30.9]	72.5 [69.7–75.4]	27.5	17.5
12	0.0 ($\delta = \pi/2$)	0.34	12.3 [6.5–18.2]	0.0 [0.0–4.3]	45.0 [41.3–48.7]	6.5	36.2
13	0.0 ($\delta = \pi/2$)	0.49	8.4 [5.6–11.1]	0.0 [0.0–5.5]	45.0 [30.1–59.9]	11.6	23.4
14	0.0 ($\delta = \pi/2$)	0.71	10.2 [3.2–16.5]	23.0 [14.6–28.7]	0.0 [0.0–3.8]	23.0	<u>9.6</u>
	Conformity number			9	2	12	7

7. Conclusions

1. It follows from the test results obtained by different authors that under combined bending with torsion and tension-compression with torsion and proportional loading, the fatigue fracture plane orientation in steels and cast irons agrees with the mean direction of the maximum normal stress or the maximum parameter of normal strain energy density, independently on the ratio of shear stresses to normal stresses λ_σ . Under non-proportional loading, the fatigue fracture plane position is dependent on the stress ratio λ_σ and the cross correlation coefficient between these stresses $r_{\sigma\tau}$.
2. In 18G2A steel, under all combinations of proportional and non-proportional loading for $\lambda_\sigma < 0.7$ the authors found only one direction of fatigue crack and two different fatigue crack directions for $\lambda_\sigma > 0.7$.
3. Under cyclic non-proportional loading ($\delta = \pi/2$), the calculation results for critical plane positions obtained with the weight function method are more close to the experimental results in comparison with the results obtained with the maximum value of selected energy parameter. Thus, we can state that in the steel tested under stresses shifted by $\delta = \pi/2$, the fatigue crack direction is connected with the mean weighed directions of principal stresses. Depending on the stress amplitude ratio λ_σ , it is the mean direction of the maximum principal or shear stress.
4. Under random loading, in the case of the maximum stress ratio $\lambda_\sigma = 0.97$ and zero correlation between stresses, $r_{\sigma\tau} = 0.0$ the pictures of the fatigue cracks (Fig. 16.a) show two crack directions and one of them is dominating.
5. The fatigue fracture plane position does not always agree with the expected critical plane positions in the verified criteria of multiaxial fatigue. Crack initiation sometimes takes place in the plane of maximum parameter of shear strain energy density and that period is a greater part of the material lifetime; during crack propagation, the fatigue fracture plane direction is influenced by the direction of the maximum parameter of normal strain energy density. Such situation was observed in 18G2A steel under non-proportional random bending with torsion and stress correlation coefficient $r_{\sigma\tau} = 0$ as well as the maximum stress ratio $\lambda_\sigma = 0.97$. At first, the crack coincided with the direction of the maximum parameter of shear strain energy density; next, the crack was branched off and propagated according to the averaged direction of the maximum principal stress.

With the support of the Commission of the European Communities under the FP5, GROWTH Programme, contract No. GIMA-CT-2002-04058 (CESTI).

Manuscript received by Editorial Board, December 04, 2003;
final version, October 14, 2004.

REFERENCES

- [1] Stanfield G.: Discussion on "The strength of metals under combined alternating stresses", by H. Gough and H. Pollard. Proc. Institution of Mechanical Engineers 131, 1935, p. 93.
- [2] Carpinteri A., Macha E., Brighenti R., Spagnoli A.: Expected principal stress directions under multiaxial random loading. Part I: Theoretical aspects of the weight function method, *Int. J. Fatigue* 21, 1999, pp. 83+88.
- [3] Carpinteri A., Macha E., Brighenti R., Spagnoli A.: Expected principal stress directions under multiaxial random loading. Part II: Numerical simulation and experimental assessment through the weight function method, *Int. J. Fatigue* 21 1999, pp. 89+96.
- [4] Macha E.: Simulation investigations of the position of fatigue plane in materials with biaxial loads, *Mat. -wiss. U. Werkstotech.* No. 20, 1989, Teil I, Heft 4/89, pp. 132+136, Teil II, Heft 5/89, pp. 153+163.
- [5] Macha E.: Generalization of strain criteria of multiaxial cyclic fatigue to random loading, *aFortschr.-Ber. VDI Reihe 18, Nr 52, VDI-Verlag, Dusseldorf* 1988, ps 102.
- [6] Findley W.N.: A theory for the effect of mean stress on fatigue of metals under combined torsion and axial load or bending, *Journal of Engineering for Industry*, November 1959, pp. 301+306.
- [7] Li J., Zhang X., Recho N.: Investigation into the growth directions of a ductile crack under tensile loading, *Journal of Theoretical and Applied Mechanics*, 4, 37, 1999, pp. 779+798.
- [8] McDiarmid D.L.: Fatigue under out-of-phase bending and torsion, *Fatigue Fract. Engng Mater. Struct.*, 9, 1987, pp. 457+475.
- [9] Munday E.G.: Significance of the relative orientation of the mean and alternating principal stress axes in biaxial fatigue, *Transaction of ASME, Journal of Engineering Materials and Technology*, Vol. 114, October 1992, pp. 406+408.
- [10] Pitoiset X., Rychlik I., Preumont A.: Spectral methods to estimate local multiaxial fatigue failure for structures undergoing random vibrations, *Fatigue Fract. Engng. Mater. Struct.*, 24, 2001, pp. 715+727.
- [11] Zamrik S.Y., Frishmuth R.E.: The effect of out-of-phase biaxial-strain cycling on low-cycle fatigue, *Experimental Mechanics*, May 1973, pp. 204+208.
- [12] Łagoda T., Macha E., Będkowski W.: A critical plane approach based on energy concepts: Application to biaxial random tension-compression high-cycle fatigue regime, *Int. J. Fatigue* 21, 1999, pp. 431+443.
- [13] Neugebauer J.: Fatigue strength of cast iron materials under multiaxial stresses of different frequencies, Report FB-175 Fraunhofer Institute fur Betriebsfestigkeit (LBF), Darmstadt, 1986.
- [14] Nishihara T., Kawamoto M.: The strength of metals under combined alternating bending and torsion with phase difference. *Memories of the College of Engineering, Kyoto Imperial University*, vol. 11, no 5, 1945, pp. 85+112.

- [15] Park J., Nelson D.V.: In-phase and out-of-phase combined bending of a notched specimen, *Multiaxial Fatigue and Deformation: Testing and Prediction*, ASTM STP1387, S. Kalluri and P.J. Bonacuse, Eds, American Society for Testing and Materials, West Conshohocken, PA, 2000, pp. 246+265.
- [16] Sanetra C.: Untersuchungen zum Festigkeitsverhalten bei mehrachsiger randombeanspruchung unter Biegung und Torsion, Fakultät für Bergbau, Huttenwesen und Maschinenwesen der Technischen Universität Clausthal, Dissertation, Berlin, 1991, ps 151.

Plaszczyzny krytyczne i złomu zmęczeniowego przy wieloosiowych obciążeniach cyklicznych i losowych

Streszczenie

W pracy położenia płaszczyzn krytycznych wyznaczone przez maksymalne wartości parametrów gęstości energii odkształcenia normalnego lub postaciowego oraz przez metodę funkcji wagowych porównano z położeniami płaszczyzn złomu wyznaczonymi eksperymentalnie. Parametry gęstości energii odkształcenia normalnego i postaciowego stosowane w kryteriach: (i) kryterium maksymalnego parametru gęstości energii odkształcenia normalnego w płaszczyźnie krytycznej i (ii) kryterium maksymalnego parametru gęstości energii odkształcenia postaciowego w płaszczyźnie krytycznej zostały użyte do wyznaczenia położenia płaszczyzn krytycznych. W metodzie drugiej funkcje wagowe sformułowano na podstawie parametrów energetycznych. Obydwie metody zostały poddane weryfikacji na podstawie danych eksperymentalnych otrzymanych z testów zmęczeniowych stali 18G2A przy losowym zginaniu, skręcaniu oraz kombinacji zginania ze skręcaniem przy różnych współczynnikach korelacji wzajemnej naprężeń normalnych i stycznych. Uzyskano zadowalającą zgodność wyników obliczeń według obu metod z danymi eksperymentalnymi.